American Mineralogist, Volume 96, pages 1392–1397, 2011

Calibration for IR measurements of OH in apatite

KAREN L. WANG,[1] YOUXUE ZHANG,[1,*] AND FABIAN U. NAAB[2]

[1]Department of Geological Sciences, University of Michigan, Ann Arbor, Michigan 48109, U.S.A.
[2]Department of Nuclear Engineering and Radiological Sciences, University of Michigan, Ann Arbor, Michigan 48109, U.S.A.

ABSTRACT

In this work, we have calibrated the infrared (IR) method for determining OH concentrations in apatite with absolute concentrations obtained through elastic recoil detection (ERD) analysis. IR spectra were collected on oriented, single-crystal apatite samples using polarized transmission infrared spectroscopy. The weight percent H_2O is 0.001199 ± 0.000029 (the error is given at 1σ level hereafter) times A/d, where A is the linear absorbance peak height measured using polarized IR when the light vector **E** is parallel to the **c**-axis of the apatite crystal, and d is the sample thickness in centimeters. This corresponds to a linear molar absorptivity, $\varepsilon = 470 \pm 11$ L/mol/cm^{-1}. The calibration using linear absorbance can be applied when there is only one dominant peak at 3540 cm^{-1}. If other peaks are significant, then the integrated molar absorptivity, $\varepsilon = (2.31 \pm 0.06) \times 10^4$ L/mol/cm^2, should be used. The detection limit of H_2O concentration in apatite by IR approaches parts per million level for wafers of 0.1 mm thickness. The accuracy based on our calibration is 5–10% relative.

Keywords: Apatite, water concentration, IR spectroscopy, ERD analysis

INTRODUCTION

Apatite is a common accessory mineral in igneous rocks on Earth, Moon (e.g., Boyce et al. 2010; McCubbin et al. 2010), and Mars (e.g., McCubbin and Nekvasil 2008). Its general formula is often written as $M_5(ZO_4)_3X$, where the M-site holds large cations such as Ca^{2+}, Sr^{2+}, and Pb^{2+}, the Z-site is usually occupied by P but can also hold As, Si, C, or S (with appropriate charge-balance substitutions), and the X-site is most commonly filled by F, Cl, and OH. The amounts of F, Cl, OH, C, and S in apatite can indicate fluid conditions during crystal formation (e.g., Mathez and Webster 2005; Boyce and Hervig 2009; Webster et al. 2009). Specifically, OH in igneous apatite can be a measure of water concentration (e.g., Boyce et al. 2010). Previously, OH concentration in apatite (typically expressed as H_2O wt% or parts per million) has been estimated by combining electron microprobe analyses of F and Cl with knowledge of mineral stoichiometry (e.g., Mathez and Webster 2005; McCubbin and Nekvasil 2008). However, the X-ray intensity for the F$K\alpha$ peaks when analyzing apatite varies as a function of electron beam exposure time and crystallographic orientation (Stormer et al. 1993; Henderson et al. 2010), which also adversely affects the detection limit of OH. Recently, SIMS has also been applied to measure H content in apatite (Boyce et al. 2010; McCubbin et al. 2010).

Fourier transform infrared spectroscopy (FTIR) can detect the OH fundamental stretching peaks in apatite at ~3540 cm^{-1} (e.g., Bhatnaga 1967; Levitt and Condrate 1970; Tacker 2004) with potentially high spatial resolution (routinely 50×50 μm with a microscope attachment, and possibly 20×20 μm) and high sensitivity. However, the absorption bands only indicate the relative concentration of OH. To determine absolute OH concentration, a calibration of the IR method using an independent method for determining absolute concentration is needed. One method for determining the absolute water concentration is extraction of H_2O (e.g., Nadeau et al. 1999). This method requires picking a large quantity of inclusion-free apatite fragments, which is often prohibitively difficult. Another method is elastic recoil detection (ERD) (e.g., Aubaud et al. 2009; Bureau et al. 2009; Cherniak et al. 2010), a surface method that can determine absolute H concentration in a surface layer of about 400 nm, but requires large sample size (>4 mm diameter, at the University of Michigan Ion Beam Laboratory). That is, the ERD method cannot be applied to analyze small apatite crystals, such as those found as accessory minerals in typical igneous rocks.

In this work, we present a calibration for absorbance measurements of OH by analyzing large, gem-quality, apatite crystals using both FTIR and ERD. With the calibration, absolute water concentration of small apatite crystals can be determined to high accuracy using polarized FTIR.

SAMPLES AND ANALYTICAL METHODS

Samples

Five large, gem-quality, single-crystal apatite samples were obtained from various localities: Durango, Mexico (two crystals labeled DurMex and Cerro); High Atlas Mountains, Morocco (HAM); and two crystals of unknown locality purchased from an online vendor (Gem3 and Gem4). All were light yellow green and transparent before polishing. A large crystal from Silver Crater Mine, which was not of gem quality was also analyzed, but the results are not used (see discussion below).

DurMex was originally ~6 mm in diameter and ~15 mm long, with visible fluid inclusions. When viewed under a microscope at 10× magnification, the

* E-mail: youxue@umich.edu

inclusions appeared to be in linear strings (possibly the result of planar healed fractures). These areas were avoided during FTIR analysis. Due to their placement, we were unable to avoid the inclusions during ERD analysis. However, because of their small size, and the low penetration depth (400 nm) of the ion beam, we do not think the ERD analysis was affected by the presence of the inclusions.

Cerro was originally ~15 mm in diameter and ~18 mm long. The sample has no visible inclusions, even under high magnification. When cut, visible internal fractures along the **c**-axis were observed. These were avoided during both ERD and FTIR analyses.

HAM was originally ~17 mm in diameter and ~18 mm long. Small (≤1 mm diameter) brown and black inclusions were visible with the naked eye, and wafers were cut to avoid these inclusions. Similar to Cerro, visible internal fractures along the **c**-axis were observed after cutting, which were avoided during FTIR and ERD analyses.

Gem3 and Gem4 were from a batch of gem apatite crystals from an online vendor. Gem3 was originally ~7 mm in diameter and ~10 mm long. Microfractures were apparent in polished wafers, which may have resulted from either the cutting or polishing processes. Gem4 was originally ~6 mm in diameter and ~8 mm long. Internal cracks and large (~1 mm long) inclusions were apparent to the naked eye. Inclusions were polished away so that surfaces were flat for both ERD and FTIR analyses.

All samples were mounted on glass with Crystalbond for cutting and polishing. Samples were then cleaned with acetone and ethanol, and placed in a vacuum desiccator before analysis.

ERD analyses

All ERD analyses were carried out at the Michigan Ion Beam Laboratory at the University of Michigan with the 1.7 MV Tandetron accelerator. The instrument setup is similar to that discussed by Aubaud et al. (2009) and Bureau et al. (2009). In an ERD analysis, a beam of high-energy ions strikes the sample and knocks off H ions. Some recoiled H ions will escape from the incident surface to be recorded by detectors. In this study a 2 MeV He^{++} ion beam was used. This energy allows us to analyze the hydrogen content in the sample to a depth of ~400 nm. Two detectors simultaneously collect the ERD and Rutherford back-scattering (RBS) spectra. The RBS spectrum is used to measure the number of particles incident on the sample during the acquisition of the ERD spectrum. An 8 µm Mylar film was used in front of the ERD detector to filter out ions heavier than hydrogen and a Kapton ($H_{10}C_{22}N_2O_5$) foil was used as the hydrogen standard to determine the ERD detector solid angle ($\Delta\Omega$) (Wang 2004). No additional calibration or standards are needed to determine absolute hydrogen concentration using the ERD method (Tirira et al. 1991; Aubaud et al. 2009; Bureau et al. 2009).

Apatite wafers were polished with SiC sandpaper and 0.3 µm alumina powder on cloth. The Cerro sample was coated with a Ni film a few nanometers thick to prevent charge build up during ion beam analysis because it was observed to spark during initial trials of ERD analysis. No other samples required such coating.

Atomic hydrogen concentration was determined through ERD and RBS spectrum modeling using the SIMNRA program (Mayer 1999). Some samples were run multiple times, with separate runs being modeled independently.

FTIR spectroscopy

Polarized IR spectra were acquired with a Perkin-Elmer Spectrum GX FTIR spectrometer using the microscope attachment, purged with N_2 gas. Instrument parameters for most runs were as follows: infrared source, KBr beamsplitter, KRS-5 IR wire grid polarizer for microscope, liquid nitrogen cooled MCT detector, 1 cm^{-1} resolution, IR range of 7800–400 cm^{-1}, and 50 × 50 µm aperture. Levitt and Condrate (1970) showed that the OH stretch band in apatite is not excited when the light vector **E** is perpendicular to the crystallographic **c**-axis, and maximum absorption occurs when **E** is parallel to **c**. Hence, samples were oriented and measured in polarized, transmitted light, following the procedure of Levitt and Condrate (1970). In some cases, very small samples were placed on a KBr disk for analysis.

Apatite sections were cut parallel to the **c**-axis with a diamond wafering saw, and doubly polished with SiC sandpaper and 0.3 µm alumina powder on cloth. Because the OH absorption band can be intense, samples were thinned down until absorbance over sample thickness was found to be constant after subsequent thinning. For our FTIR polarizer and microscope setup, this has been observed to occur when peak heights are lower than ~1.3 absorbance units. As H_2O concentration increases, the required thickness decreases. The thinnest wafer in this study has a thickness of about 14 µm. Some sample thicknesses (especially the thin samples) were determined using interference fringes between 3400–2100 cm^{-1}. Since values for index of refraction may vary with composition, $n = 1.65 \pm 0.01$ was used. Thicknesses determined from interference fringes were compared with directly measured thicknesses using a Mitutoyo digital micrometer (with an uncertainty of ±2 µm), and were in agreement within error, justifying the use of refractive index values for visible light wavelengths in the absence of refractive indices at 3400–2100 cm^{-1}. For samples where interference fringes were not present or not clean, thicknesses were measured on multiple spots using the micrometer.

Maximum linear absorbance peak height of the 3540 cm^{-1} band (OH stretch) and integrated absorbance area between 3670–3300 cm^{-1} were determined with the Spectrum program. Absorbance values were corrected against a linear baseline in all cases.

RESULTS

ERD analyses

Figure 1 shows selected ERD spectra for each sample. Actual counts are shown on the right vertical axis, and counts normalized by the number of incident ions are shown on the left vertical axis. With the normalized counts, the "plateau" height is proportional to relative H concentration. Channel number denotes energy of the hydrogen ions detected by the ERD detector; higher channel number corresponds to higher energy. The energy of the detected hydrogen ion is related to the original depth of the hydrogen atom in the sample. Hydrogen ions from the surface of the samples have the highest energy. Therefore, channel number is also a proxy for shallowness; depth increases with decreasing channel number. The large peak at high channel numbers dominating each spectrum is the surface peak, commonly seen in ERD spectra (e.g., Bureau et al. 2009). This feature is attributed to adsorbed H. Hydrogen concentration is determined by modeling the inner "plateau" height (typically between channel numbers 50 and 160; Fig. 1). Note that although we refer to it as a plateau for simplicity, there is a small slope to it (as can be seen from the data and model curve) at constant concentration due to larger energy dispersion for H ions from greater depth, meaning less counts at smaller channel numbers. This effect is modeled by the SIMNRA program. Table 1 lists all modeled atomic percents (at%) of H, as well as the corresponding calculated wt% H_2O. Original and modeled digital ERD spectra can be found in supplementary data[1].

Errors in the ERD method are discussed in Aubaud et al. (2009) and Bureau et al. (2009). The largest uncertainty comes from the statistical count rate. With ≤10 counts per channel and ~100 channels within the inner plateau, errors can reach 5–10%. There are also uncertainties involved when using the SIMNRA program to model the H concentration. Hence, the total uncertainty is larger than that based on counting statistics. For four of the five samples, multiple ERD measurements were made. The reproducibility error is often larger than the calculated error based on counting statistics. The reproducibility of multiple measurements is a better measure of the error and hence is used as the uncertainty for the calibration.

[1] Deposit item AM-11-043, original data. Deposit items are available two ways: For a paper copy contact the Business Office of the Mineralogical Society of America (see inside front cover of recent issue) for price information. For an electronic copy visit the MSA web site at http://www.minsocam.org, go to the *American Mineralogist* Contents, find the table of contents for the specific volume/issue wanted, and then click on the deposit link there.

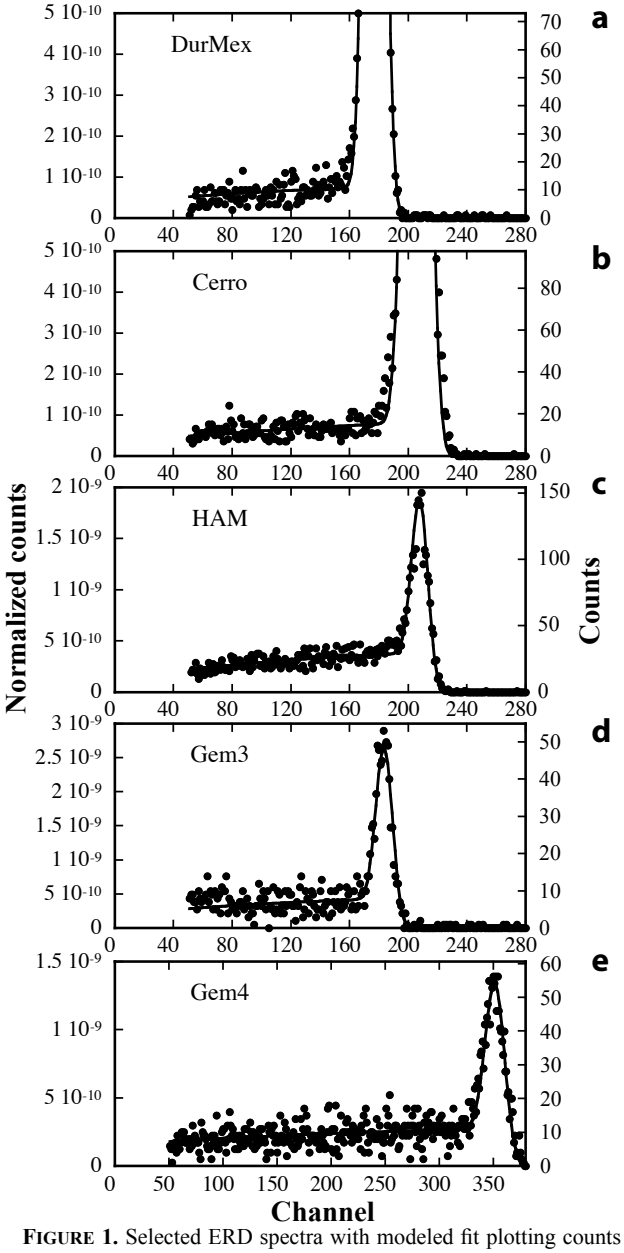

FIGURE 1. Selected ERD spectra with modeled fit plotting counts normalized by number of incident ions, and raw counts, against channel number (a proxy for shallowness into sample) for samples from (**a**–**b**) Durango, Mexico; (**c**) High Atlas Mountains, Morocco; (**d**–**e**) unknown locality, from an online vendor. The strong peak at high channel numbers is the surface peak, attributed to adsorbed H. Corresponding at% H values are obtained using the SIMNRA program.

FTIR spectroscopy

All five samples showed maximum peak height at the same wavenumber (3540 cm^{-1}) and a single dominant peak (Fig. 2). Table 2 summarizes the absorbance data. Both linear peak height and integrated peak area between 3670–3300 cm^{-1} were used for absorbance values in this calibration. The calibration using linear peak heights are for the convenience of users to rapidly estimate H_2O content in apatite. Because when **E**⊥**c**, the absorbance (either linear or integrated) cannot be resolved from the noise and is essentially zero, the measured absorbance at **E**//**c** is also the total absorbance summed along three principal directions.

An apatite crystal from Silver Crater Mine was also analyzed. The crystal was not gem-quality and was gray in color. Although the sample was transparent at its polished thickness of <20 μm, numerous inclusions and imperfections were still apparent. The sample was analyzed using both ERD and FTIR. ERD showed 1.24 at% H (0.465 wt% H_2O), but FTIR measurements on several points avoiding inclusions and imperfections showed a very small OH peak, partially hidden within noise, which would correspond to ~0.04 wt% H_2O using our calibration. The inconsistency is attributed to inhomogeneity of the crystal and presence of small inclusions. Hence, this sample was not used in the calibration.

Due to the anisotropic properties of apatite, the accurate orientation of crystals during FTIR analysis is essential. Additional FTIR analysis was done on HAM, changing the polarizer in 10° increments (Fig. 3a). The data show that with the **E**-vector perpendicular to the **c**-axis, absorbance is 0 (Fig. 3b). Figure 3 verifies the dependence of absorbance values on the angle between the **E**-vector and the crystallographic **c**-axis, which follows the formula given in Strens et al. (1982) and Libowitzky and Rossman (1996). Improper orientation of the polarizer relative to the crystal is thus an important factor in the error of IR absorbance values, since there is a relatively steep absorbance difference with a small change in angle near the maximum. For our polarizer, each notch of the polarizer angle adjustment is 5°, meaning the error is ≤2.5°. This translates into a calculated relative error of 1% in the maximum peak height at **E**//**c** for the examples in Figure 3a. Some polarizers may not be able to reproduce the zero absorbance for **E**⊥**c** due to inefficiency of the polarization. Original FTIR data, including spectra with **E**⊥**c** can be found in supplementary data[1].

Two other sources of error to consider in FTIR measurements are the choice of baseline when correcting spectra and the measurement of sample thickness. A linear baseline is used in all the absorbance values of this study. Typical uncertainty in A is ±0.001 absorbance units. However, larger errors can occur

TABLE 1. ERD data for H at% and corresponding wt% H_2O in five apatite crystals

	DurMex	Cerro	HAM	Gem3	Gem4
H (at%)	0.23 ± 0.008	0.21 ± 0.010	1.13 ± 0.032	1.3 ± 0.05	1.15 ± 0.07
		0.25 ± 0.007	1.15 ± 0.046	1.6 ± 0.06	1.20 ± 0.05
			1.17 ± 0.022	1.7 ± 0.12	1.25 ± 0.04
			1.20 ± 0.060		1.59 ± 0.03
H_2O (wt%)	0.086 ± 0.003	0.075 ± 0.004	0.430 ± 0.012	0.495 ± 0.019	0.435 ± 0.026
		0.095 ± 0.003	0.435 ± 0.017	0.607 ± 0.022	0.455 ± 0.019
			0.440 ± 0.008	0.644 ± 0.046	0.480 ± 0.015
			0.455 ± 0.023		0.607 ± 0.012
Avg. H_2O (wt%)	0.086 ± 0.003	0.085 ± 0.014	0.440 ± 0.011	0.582 ± 0.078	0.494 ±0.077

Notes: Each entry represents a repeated measurement. Errors in at% H represent counting statistics, with relative error calculated as $1/\sqrt{n}$. Average H_2O in wt% is based on simple reproducibility (not weighted average) for samples that were measured multiple times.

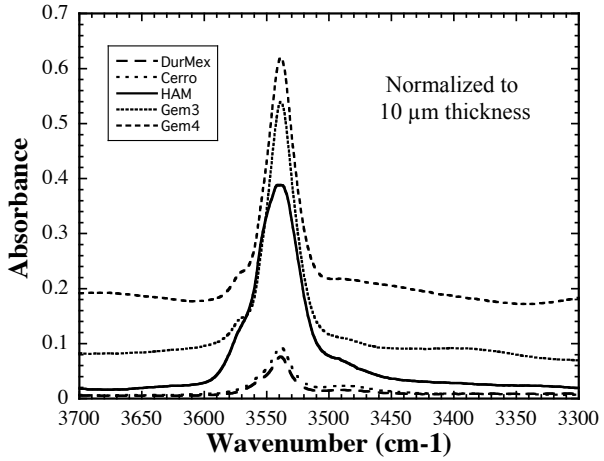

FIGURE 2. Selected IR spectra for each of the five samples of the OH stretch absorption band when the light vector **E** is parallel to the crystallographic **c**-axis. Data has been normalized to 10 μm thickness and offset for comparison.

TABLE 2. FTIR measurements

	DurMex	Cerro	HAM	Gem3	Gem4
d (μm)	59 ± 2	59.8 57.3 61.1 61.1 58.7	32.5; 32.6; 32.9; 31.9; 32.3; 32.3; 32.0; 32.8; 33.2	16.9; 19.7; 21.6; 23.8; 16.0; 21.2	27.0; 14.2; 13.3; 13.6; 13.3; 12.8
A_{Lin}	0.414 ± 0.027	0.541 0.520 0.550 0.547 0.528	1.191; 1.190; 1.219; 1.192; 1.188; 1.157; 1.092; 1.109; 1.101	0.833; 0.922; 1.016; 1.046; 0.786; 0.966	1.067; 0.667; 0.597; 0.616; 0.633; 0.601
Avg. A_{Lin}/d (d in cm)	70.1 ± 5.2	90.1 ± 0.5	357 ± 16	470 ± 20	451 ± 30
A_{Int}	13.9 ± 1.8	23.0 22.8 23.6 23.5 22.9	63.2; 61.8; 62.6; 61.8; 63.5; 62.6; 59.4; 62.1; 60.5	33.9; 32.8; 37.3; 38.4; 24.7; 38.4	39.6; 19.8; 20.0; 26.0; 20.6; 22.5
Avg. A_{Int}/d (d in cm)	2363 ± 315	3888 ± 55	19067 ± 471	17286 ± 1663	15935 ± 1961

Notes: A_{Lin} means linear absorbance. A_{Int} means integrated absorbance (area). Errors are given at 1σ level. For DurMex, the error in A represents deviation of repeated IR measurements, the error in thickness is due to the digital micrometer (interference fringes are not clear for this sample); and the error in A/d is based on error propagation. For Cerro, Ham, Gem3, and Gem4, errors in A/d are based on multiple IR measurements with both thickness (from interference fringes) and absorbance from IR spectra.

when absorbance peak height is comparable to the amplitude of interference fringes. This can also complicate the interpretation of interference fringes when determining sample thickness.

During early FTIR analyses, it was observed that choice of aperture size had an effect on the absorption band intensity. Notably, absorbances were lower when the aperture size was reduced from 300 × 300 to 100 × 100 μm. However, band intensities were within error for aperture sizes of 50 × 50, 40 × 40, and 30 × 30 μm. Therefore, to avoid additional error, we recommend using only aperture sizes equal to or smaller than 50 × 50 μm when using this calibration.

Other peaks can also be seen in IR spectra. In particular, the CO_3^{2-} double peaks around 1500–1350 cm^{-1} (also at 870 cm^{-1}, though not shown; e.g., Fleet and Liu 2008) are observed to change with the angle of polarized light (Fig. 4). The double

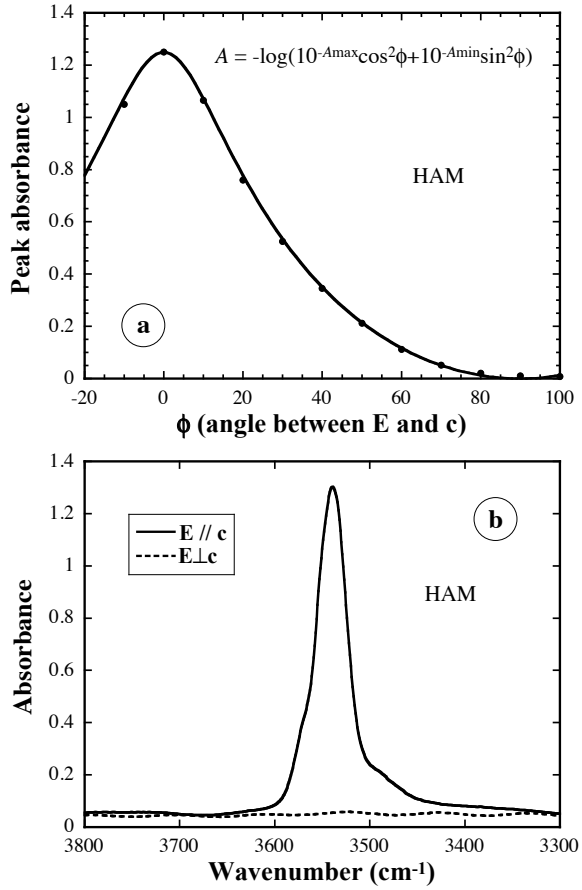

FIGURE 3. (**a**) Variation in absorbance with the angle between **E**-vector of polarized light and the crystallographic **c**-axis. Diamonds show measured absorbance peak heights from HAM, solid line is the calculated theoretical absorbance value following: $A(\varphi) = -\log(10^{-A_{max}}\cos^2\varphi + 10^{-A_{min}}\sin^2\varphi)$, where φ is the angle between the **E**-vector and the **c**-axis. (**b**) FTIR spectra for HAM of the OH stretch absorption band for **E**//**c** and **E**⊥**c**, showing that absorbance is 0 when **E** is perpendicular to the **c**-axis.

peaks are the most uneven when the **E**-vector is parallel to the crystallographic **c**-axis, and approach similar peak heights when the **E**-vector is perpendicular to **c**.

Calibration

Based on Beer's law, H_2O concentration in apatite can be related to measured IR absorbance as follows:

$$C = \frac{wA}{\varepsilon\rho d} \quad (1)$$

where C is H_2O mass fraction (C = 0.01 for 1 wt% H_2O), w = 18.015 g/mol is the molar mass of H_2O, A is either total linear peak height (A_{Lin}) or total integrated absorbance (A_{Int}) of the IR band, d is the thickness of the sample, ρ is the density of apatite (3200 g/L), and ε is the molar absorptivity. The "total" means summing absorbances along three principal directions of apatite. Because the absorbance is essentially zero for **E**⊥**c**, the total absorbace is the same as the absorbance at **E**//**c**. Or simply, the concentration is proportional to absorbance per unit thickness (A/d).

Based on Equation 1, plotting H_2O concentration against

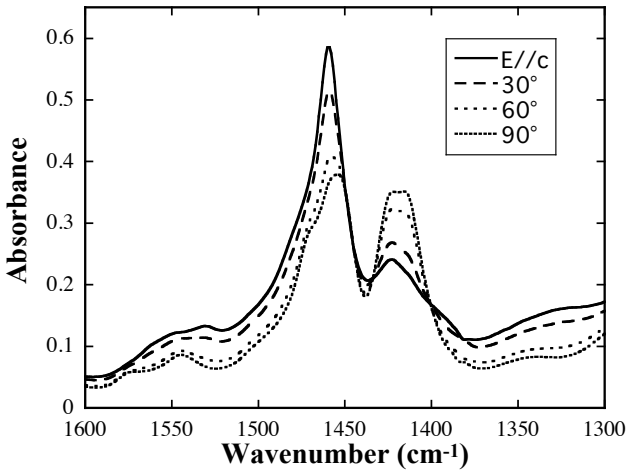

FIGURE 4. Variation in CO_3^{2-} absorbance in HAM sample due to angular alignment of polarized light with the crystallographic **c**-axis (angle denotes change from **c**-axis direction). The two bands approach similar peak heights when **E** is perpendicular to the **c**-axis.

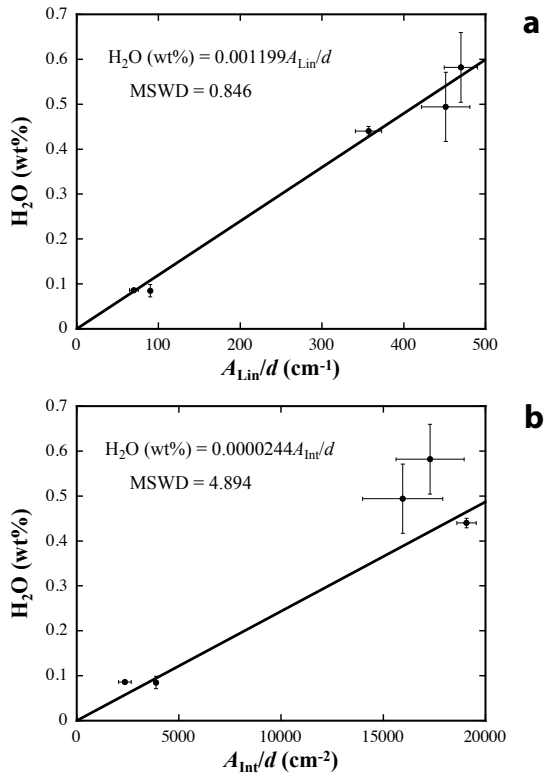

FIGURE 5. Calibration line for IR measurements of OH in apatite, where (**a**) A_{Lin} is linear absorbance peak height ~3540 cm^{-1} and (**b**) A_{Int} is integrated absorbance between 3670–3300 cm^{-1}. Average wt% H_2O values are plotted on the vertical axis. Error bars are shown at 1σ level.

A/d is a straight line. Figure 5a shows the relation between H_2O concentration determined from ERD and A_{Lin}/d. The data are fit using a modified York algorithm (York 1969) constrained to have an intercept of zero (Chris Hall, personal communication). We find that the weight percent of H_2O is 0.001199 ± 0.000029 times A_{Lin}/d, where d is in centimeters. The mean square weighted deviation (MSWD) is 0.8459, indicating a good fit since MSWD < 1. The corresponding molar absorptivity is $\varepsilon_{Lin} = 470 \pm 11$ L/mol/cm^{-1}. Using the integrated absorbance, the weight percent of H_2O is about 2.44×10^{-5} times A_{Int}/d with MSWD = 4.894 (Fig. 5b). The reason for this less-than-satisfactory fit as indicated by the large MSWD value is not known. The corresponding molar absorptivity is $\varepsilon_{Int} \approx 2.31 \times 10^4$ L/mol/cm^2.

DISCUSSION

Comparison of different techniques

There are now five different methods to analyze OH content in apatite: (1) electron microprobe and stoichiometry, (2) extraction and manometry, (3) ERD, (4) IR, and (5) SIMS. The electron microprobe analysis coupled with stoichiometry cannot provide accurate OH concentrations (see introduction above). H_2O extraction and manometry are an absolute method but require hand picking a large quantity of inclusion-free apatite fragments. For ERD, the main advantage is that it is an absolute method that does not require external calibration. The disadvantages include the (1) large sample size requirements, (2) inability to distinguish among different forms of H, and (3) high detection limit (>100 ppm H_2O).

The major advantages of the IR method lie in the ability to determine the hydrogen species (e.g., SIMS and ERD methods can detect total H, but cannot determine whether H is present as OH or some other form), the ability to measure small samples, the precision and accuracy, and the low detection limit (~1 ppm for a sample of 0.1 mm thickness based on typical IR spectrum noise level of about 0.001 absorbance units). Furthermore, FTIR is widely available, and the method is non-destructive so that the sample may be analyzed using other methods after FTIR analysis. The main disadvantages are that the sample must be oriented and doubly polished.

The SIMS method uses a microbeam of ions. The main advantages of SIMS are that it can measure small samples with adequate detection limit, there is no need to orient the sample, and only one side needs to be polished. The disadvantages are that it cannot distinguish different forms of H, and the detection limit is about 10 ppm (based on data in Boyce et al. 2010), an order of magnitude worse than that for IR. Furthermore, SIMS is not as widely available as FTIR.

Comparison of molar absorptivities with other minerals

When comparing molar absorptivities for OH in apatite with those in glasses and other minerals, it is necessary to use those based on total absorbance (summation of absorbances from polarized spectra in all three principal directions) (Libowitzky and Rossman 1996). Because absorbance is zero in the two principal directions when **E**⊥**c** for apatite (Fig. 3), the absorbance at **E**//**c** is the total absorbance. For glasses and isotropic minerals such as garnet, the total absorbance is three times the absorbance along a given direction, and hence the molar absorptivity based on total absorbance is three times the molar absorptivity based on absorbance along any one direction.

Aubaud et al. (2009) used ERD to determine molar absorptivities for olivine (ε_{Int} = 34 515 L/mol/cm^2, where total absorbance by adding absorbances from 3 principal axes was used)

and clinopyroxene (ε_{Int} = 46 103 L/mol/cm^2). Bell et al. (1995) estimated the integrated molar absorptivity of garnet to be $3\varepsilon_{Int}$ = 20 100 L/mol/cm^2. The molar absorptivity for OH in apatite from this study (ε_{Int} = 23 100 L/mol/cm^2) is on the same order of magnitude. We can also compare our linear molar absorptivity for apatite (ε_{Lin} = 470 L/mol/cm^2) with that of rhyolitic glass based on total absorbance ($3\varepsilon_{Lin}$ = 264 to 300 L/mol/cm^{-1}; Newman et al. 1986; Dobson et al. 1989; Aubaud et al. 2009), and we again find that they fall in the same order of magnitude.

Applications

This calibration can be applied to measure absolute water concentration in apatite crystals using polarized FTIR. Due to the ubiquitous presence of apatite in igneous and metamorphic rocks, and in terrestrial, lunar, and martian rocks, and because it is important to know OH contents in apatite to constrain the formation conditions, our IR calibration is expected to find widespread use. New data will provide better understanding of volatile environments in which apatite formed, as close to home as terrestrial magma chambers and as far-ranging as lunar formation.

Furthermore, apatite may incorporate various volatile components (H_2O, CO_2, SO_3, F, Cl). Combined with electron microprobe analyses to obtain major elements, and F and Cl concentrations (Stormer et al. 1993; Henderson et al. 2010), as well as future development of FTIR for carbonate in apatite, apatite may become the most important mineral in studying volatile conditions of magma.

Acknowledgments

We thank George Rossman and an anonymous reviewer for providing constructive and careful review, Eric Essene for his help in locating high-quality apatite crystals, Chris Hall for providing the modified York linear regression program for the case of zero intercept, and Artur Deditius and Bernard Evans for providing apatite samples and data. This research is supported by NASA (NNX10AH74G) and NSF (EAR-0838127 and EAR-1019440).

References cited

Aubaud, C., Bureau, H., Raepsaet, C., Khodja, H., Withers, A.C., Hirschmann, M.M., and Bell, D.R. (2009) Calibration of the infrared molar absorption coefficients for H in olivine, clinopyroxene and rhyolitic glass by elastic recoil detection analysis. Chemical Geology, 262, 78–86.

Bell, D.R., Ihinger, P.D., and Rossman, G.R. (1995) Quantitative-analysis of trace OH in garnet and pyroxenes. American Mineralogist, 80, 465–474.

Bhatnaga, V.M. (1967) Infra-red spectrum of an apatite from Wilberforce Ontario Canada. Archives of Oral Biology, 12, 429–430.

Boyce, J.W. and Hervig, R.L. (2009) Apatite as a monitor of late-stage magmatic processes at Volcan Irazú, Costa Rica. Contributions to Mineralogy and Petrology, 157, 135–145.

Boyce, J.W., Liu, Y., Rossman, G.R., Guan, Y.B., Eiler, J.M., Stolper, E.M., and Taylor, L.A. (2010) Lunar apatite with terrestrial volatile abundances. Nature, 466, 466–469.

Bureau, H., Raepsaet, C., Khodja, H., Carraro, A., and Aubaud, C. (2009) Determination of hydrogen content in geological samples using elastic recoil detection analysis (ERDA). Geochimica et Cosmochimica Acta, 73, 3311–3322.

Cherniak, D.J., Hervig, R., Koepke, J., Zhang, Y., and Zhao, D. (2010) Analytical methods in diffusion studies. In Y. Zhang and D.J. Cherniak, Eds., Diffusion in Minerals and Melts, 72, p. 107–170. Reviews in Mineralogy and Geochemistry, Mineralogical Society of America, Chantilly, Virginia.

Dobson, P.F., Epstein, S., and Stolper, E.M. (1989) Hydrogen isotope fractionation between coexisting vapor and silicate-glasses and melts at low pressure. Geochimica et Cosmochimica Acta, 53, 2723–2730.

Fleet, M.E. and Liu, X. (2008) Accommodation of the carbonate ion in fluorapatite synthesized at high pressure. American Mineralogist, 93, 1460–1469.

Henderson, C.E., Essene, E.J., Wang, K.L., and Zhang, Y. (2010) The perils of electron microprobe analysis of apatite. In: Eos 91 (AGU Fall Meeting), abstract V51C-2206.

Levitt, S.R. and Condrate, R.A. Sr. (1970) Polarized infrared spectra of hydroxyl ion in fluorapatite. Applied Spectroscopy, 24, 288–289.

Libowitzky, E. and Rossman, G.R. (1996) Principles of quantitative absorbance measurements in anisotropic crystals. Physics and Chemistry of Minerals, 23, 319–327.

Mathez, E.A. and Webster, J.D. (2005) Partitioning behavior of chlorine and fluorine in the system apatite-silicate melt-fluid. Geochimica et Cosmochimica Acta, 69, 1275–1286.

Mayer, M. (1999) SIMNRA, a simulation program for the analysis of NRA, RBS and ERDA. In J.L. Duggan, and I.L. Morgan, Eds., Application of Accelerators in Research and Industry, Pts 1 and 2, vol. 475, p. 541–544. AIP Conference Proceedings, American Institute of Physics, Melville, New York.

McCubbin, F.M. and Nekvasil, H. (2008) Maskelynite-hosted apatite in Chassigny meteorite: insights into late-stage magmatic volatile evolution in martian magmas. American Mineralogist, 93, 676–684.

McCubbin, F.M., Steele, A., Nekvasil, H., Schnieders, A., Rose, T., Fries, M., Carpenter, P.K., and Jolliff, B.L. (2010) Detection of structurally bound hydroxyl in fluorapatite from Apollo Mare basalt 15058,128 using TOF-SIMS. American Mineralogist, 95, 1141–1150.

Nadeau, S.L., Epstein, S., and Stolper, E. (1999) Hydrogen and carbon abundances and isotopic ratios in apatite from alkaline intrusive complexes, with a focus on carbonatites. Geochimica et Cosmochimica Acta, 63, 1837–1851.

Newman, S., Stolper, E.M., and Epstein, S. (1986) Measurement of water in rhyolitic glasses—calibration of an infrared spectroscopic technique. American Mineralogist, 71, 1527–1541.

Stormer, J.C., Pierson, M.L., and Tacker, R.C. (1993) Variation of F-X-ray and Cl-X-ray intensity due to anisotropic diffusion in apatite during electron-microprobe analysis. American Mineralogist, 78, 641–648.

Strens, R.G.J., Mao, H.K., and Bell, P.M. (1982) Quantitative spectra and optics of some meteoritic and terrestrial titanian clinopyroxenes. In S.K. Saxena, Ed., Advances in Physical Geochemistry, 2, p. 327–346. Springer, New York.

Tacker, R.C. (2004) Hydroxyl ordering in igneous apatite. American Mineralogist, 89, 1411–1421.

Tirira, J., Frontier, J.P., Trocellier, P., and Trouslard, P. (1991) Development of a simulation algorithm for energy spectra of elastic recoil spectrometry. Nuclear Instruments and Methods in Physics Research B, 54, 328–333.

Wang, Y.Q. (2004) Hydrogen standards in elastic recoil detection analysis. Nuclear Instruments and Methods in Physics Research B, 219–220, 115–124.

Webster, J.D., Tappen, C.M., and Mandeville, C.W. (2009) Partitioning behavior of chlorine and fluorine in the system apatite-melt-fluid. II: Felsic silicate systems at 200 MPa. Geochimica et Cosmochimica Acta, 73, 559–581.

York, D. (1969) Least-squares fitting of a straight line with correlated errors. Earth and Planetary Science Letters, 5, 320–324.

Manuscript received December 6, 2010
Manuscript accepted April 19, 2011
Manuscript handled by Grant Henderson